The Journal of Physical Chemistry A

 VOLUME 103, NUMBER 3, JANUARY 21, 1999

LETTERS

Identification of Single Molecules in Aqueous Solution by Time-Resolved Fluorescence Anisotropy

J. Schaffer, A. Volkmer, C. Eggeling, V. Subramaniam, G. Striker, and C. A. M. Seidel*

Max-Planck-Institut für Biophysikalische Chemie, Am Fassberg 11, D-37077 Göttingen, Germany

Received: August 12, 1998; In Final Form: November 23, 1998

Using a confocal epi-illuminated microscope with a polarizing beam splitter and dual-channel detection of single-molecule fluorescence induced by pulsed laser excitation, a new application of the three-dimensional, real-time spectroscopic technique BIFL (burst integrated fluorescence lifetime) is introduced. BIFL allows simultaneous registration of fluorescence intensity, lifetime, and anisotropy. It is shown to be well-suited to identify the freely diffusing fluorescent molecule Rhodamine 123 and the Enhanced Yellow Fluorescent Protein via their characteristic fluorescence anisotropy using a time-resolved analysis. Furthermore, data analysis is discussed and rotational correlation times of single molecules are determined. Applications for multidimensional single-molecule identification are outlined.

Introduction

The sensitivity of laser-induced fluorescence detection has reached levels which allow for the detection and even identification of single molecules in solution by their characteristic spectroscopic properties.[1−8] Thus, molecular recognition by an environment-sensitive fluorescent dye attached to a biomolecule opens up the opportunity to characterize specific molecular states. This recent progress in single-molecule spectroscopy is a major step toward the direct study of single-molecule dynamics.[9−11] Characteristic fluorescence properties of a single fluorophore in solution are its spectrum, quantum yield, excited-state lifetime, τ, and anisotropy.[9,11] However, only the first three properties have been exploited so far. This work presents a feasibility study to identify freely diffusing single molecules in solution by their characteristic steady-state anisotropy, r, which is determined by the rotational correlation time, ρ, and the initial anisotropy, $r(0)$, at time $t = 0$. This is experimentally achieved by use of linear polarized pulsed excitation, confocal fluorescence spectroscopy with two detectors and the recently developed, real-time BIFL-technique (burst integrated fluorescence lifetime).[4,8,10] BIFL enables the simultaneous acquisition of the three-dimensional fluorescence intensity, lifetime, and anisotropy information.

For this study, two fluorescent probe molecules were selected (see Table 1): The small fluorescent dye Rhodamine 123 (Rh 123) and the enhanced yellow mutant (EYFP) of the Green Fluorescent Protein (GFP). They have similar spectra (absorption and fluorescence maxima, $\lambda_{A,max}$ and $\lambda_{F,max}$, respectively), fluorescence quantum yield, Φ_F, lifetime, τ, and high value of $r(0)$, close to the theoretical limit of 0.4 for one-photon excitation. However, they differ by approximately 2 orders of magnitude in their rotational correlation time, ρ, which results in a significantly different steady-state anisotropy, r.

GFP has attracted enormous attention in recent years as an important reporter molecule in cell, developmental, and molecular biology.[12,13] GFP can be fused to a variety of proteins without affecting their function. These proteins are expressed in vivo and thus act as remarkably versatile indicators of structure and function within cells.[13,14] Several mutants of GFP with enhanced fluorescence properties and spectral properties

* Corresponding author. E-mail: cseidel@gwdg.de.

10.1021/jp9833597 CCC: $18.00
Published on Web 12/31/1998

TABLE 1: Optical Properties of the Fluorescent Probe Molecules in Aqueous Solution Determined by Bulk Measurements

properties	Rh 123	EYFP
$\lambda_{A,max}/\lambda_{F,max}$	502 nm/525 nm	514 nm/527 nm
Φ_F	0.95	0.63[20]
τ	4.0 ns	multiexp.; av: 3.2 ns
$r(0)$	0.37	0.39
ρ	0.20 ± 0.05 ns	16 ± 2 ns
r	0.02 ± 0.01	0.32 ± 0.01

different from that of the wild-type GFP protein have been generated,[15,16] allowing a variety of uses including spectral separation of different GFPs[17] and fluorescence resonance energy transfer.[18,19]

In this letter, we present procedures for data analysis of steady-state and time-resolved anisotropy in confocal fluorescence microscopy. On the basis of these first results obtained from individual molecules, a three-dimensional fluorescence characterization of mixtures of different fluorescent probe molecules demonstrates that the chance of misclassification is as low as 1%, if the anisotropy is used as the selection criterion.

Experimental Section

The Enhanced Yellow Fluorescent Protein (EYFP) coding sequence was cloned into the expression vector pRSETa (Invitrogen, USA) and was a gift of Dr. David Piston (Vanderbilt University, Nashville, TN). The EYFP mutant carries the following changes in the protein sequence, first reported by Ormo et al.:[20] S65G, V68L, S72A, T203Y. The recombinant protein with a 6-histidine tag was expressed and purified on a Ni-chelating resin, according to standard procedures.[21] The measurements on EYFP and Rhodamine 123 chloride (Rh 123, Sigma (Deisenhofen, Germany)) were performed in microcells (0.9 mm square i.d., VitroCom Inc. (Mt. Lakes, NJ)) using a 10 mM Na−phosphate buffer (pH = 8.7) with a solute concentration of approximately 5×10^{-12} M.

Confocal fluorescence detection was performed using an active-mode-locked argon-ion laser (Sabre, Coherent (Palo Alto, CA) and an active-mode locker, APE (Berlin, Germany), an excitation wavelength of 502 nm, a repetition rate of 73 MHz, a pulse width of 190 ps, a focal excitation irradiance of 60 kW cm^{-2}) with an epi-illuminated microscope[2,6] (water immersion objective (UPLANAPO 60×, NA = 1.2, Olympus (Tokyo, Japan)), beam-splitter at 505 nm (AHF Analyzentechnik (Tübingen, Germany)), 80 μm pinhole, and dichroic band-pass filter (HQ 535/50 nm (AHF Analyzentechnik))). After passing the pinhole, the fluorescence was divided into its parallel and perpendicular components with respect to the linear polarized excitation beam by a polarization beam-splitter cube (VISHT11, Gsänger, (Planegg, Germany)). Each component was separately detected by an avalanche photodiode (AQ 151, EG&G (Vaudreuil, Quebec, Canada)). Both output signals were processed and stored by a PC−BIFL card (either SPC 401/431, Becker & Hickl GmbH (Berlin, Germany) or SL Digital time 70 (SL Microtest, Jena, Germany)). The focal area and the detection volume of approximately 6 fl were determined by fluorescence correlation spectroscopy (radial $1/e^2$ radius of $\omega = 0.65$ μm, axial $1/e^2$ radius of $z = 2.6$ μm, and characteristic diffusion times, τ_D(Rh 123) = 0.35 ms and τ_D(EYFP) = 1.0 ms).

Results and Discussion

BIFL. Using a highly diluted aqueous sample solution and confocal fluorescence spectroscopy with polarized pulsed excitation, fluorescence bursts indicating transits of individual molecules are registered and further subjected to selective burst analysis. We applied the multidimensional BIFL technique to simultaneously record three parameters for each detected photon: (1) the polarization of the signal photon (parallel or perpendicular) with respect to the linear polarization of the exciting laser; (2) the time lag, Δt, to the preceding signal photon (millisecond time range) to enable a specific and photon-exact fluorescence burst selection; and (3) the arrival time of the signal photon relative to the incident laser pulse, measured by time-correlated single-photon counting (picosecond to nanosecond time scale). In this manner arrival time histograms are constructed only from those registered events which are within the fluorescence burst of a single-molecule transit selected from the signal trace (see Figure 1). To determine the fluorescence parameters of interest based on this small number of detected fluorescence photons, an efficient pattern recognition technique must be used as outlined below.

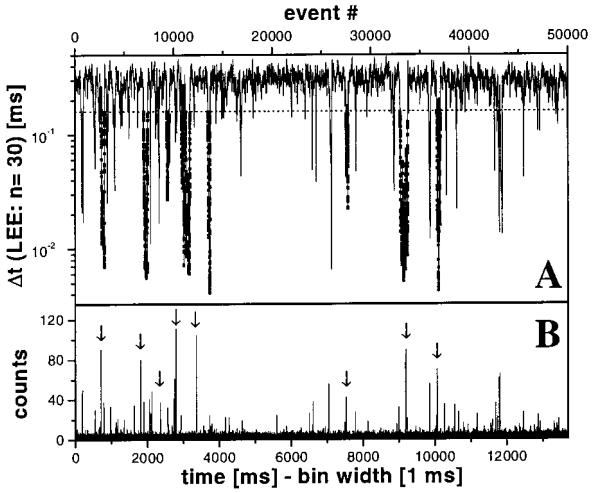

Figure 1. Two equivalent BIFL representations of a time-dependent signal trace of the dye mixture Rh 123/EYFP in buffer. (A) Time lag, Δt, between consecutive photons of the smoothed data (Lee-filtered: width, $2m + 1 = 61$, constant filter parameter, $\sigma_0 = 10^{22}$) and threshold value, $\Delta t_{th} = 0.16$ ms, for the subsequent burst selection (dashed line) versus the signal event number ((■) selected photons). (B) Multichannel scaler (MCS) trace with a bin width of 1 ms, calculated from the Δt trace of (A), versus the macroscopic measurement time of the experiment ((↓) selected bursts). The different *x*-axes of A and B reveal slight distortions in the position of related fluorescence bursts.

The lower panel of Figure 1 displays a multichannel scaler (MCS) trace of fluorescence raw data from a mixture of Rh 123 and EYFP, exhibiting distinct fluorescence bursts due to single molecule events. The number of the registered photoelectron is plotted versus the time lag, Δt, between two consecutive detected photons in the upper panel of Figure 1. Since any integration of events is avoided, a Δt trace, which has been smoothed by a Lee filter [22] (only for burst selection), allows an exact selection of the desired fluorescence photons with a time lag smaller than a threshold, $\Delta t_{th} = 0.16$ ms. To reduce statistical errors in the subsequent raw data analysis of the fluorescence parameters, bursts having a minimum size of 200 photons were selected only. Using such a sample survey technique, it is possible to identify and quantify the sample molecules in an open volume element, as reported previously.[8]

Steady-State Anisotropy. A direct measure for the time-dependent fluorescence anisotropy of a single molecule in the arrival time window, *T*, is the steady-state anisotropy, *r*, calculated by the polarized fluorescence signal, which is orientated parallel ($f_{||}(t)$) and perpendicular ($f_{\perp}(t)$) to the linear polarized laser excitation, respectively.

$$r = \frac{\int_T dt[f_{||}(t) - f_{\perp}(t)]}{\int_T dt[f_{||}(t) + 2f_{\perp}(t)]} \quad (1)$$

However, refraction by the microscope objective lenses changes the linear polarization orientation of the excitation light and fluorescence emission. Therefore, an analytical method developed by Koshioka et al.[23] is applied to describe the imaged fluorescence, $j_{||}$ and $j_{\perp}$, by the use of two correction factors, l_1 and l_2. We define the x-axis as parallel and the y-axis as perpendicular to the polarization of the exciting laser, the $x-y$ plane being coincident with the sample plane. Thus, the fluorescence collected parallel to the x-axis, which is registered by detector 1, is mixed with y- and z-axial polarized components. Similar considerations hold for detector 2, which monitors the fluorescence parallel to the y-axis. Furthermore, the slightly different detection efficiencies, $E_{||}$ and $E_{\perp}$, of the two detection systems must be taken into account by the factor $G = E_{\perp}/E_{||}$. Since the data are accumulated in k channels with a total arrival time window, $T = 13.6$ ns, the continuous time, t, in the signal decay patterns is replaced by the time, $t_i = iT/k$, of the channel, i. The experimental anisotropy, r_E, is easily calculated from the counted events, $c_{x,i}$ and $c_{y,i}$, of the channel, i, in the two signal decay histograms (eq 2).

$$r_E = \frac{G\sum_{v=1}^{k} c_{x,v} - \sum_{v=1}^{k} c_{y,v}}{(1 - 3l_2)G\sum_{v=1}^{k} c_{x,v} + (2 - 3l_1)\sum_{v=1}^{k} c_{y,v}} \quad (2)$$

It is important to note that the total registered signal contains fluorescence, j_x and j_y, and variable fractions, γ, of scattered light, s_x and s_y, which skews the calculated fluorescence anisotropy ($\gamma = (Gs_x + 2s_y)/(G(s_x + j_x) + 2(s_y + j_y))$). Taking into account an effective scatter-polarization ratio, $\alpha = 2s_y/(Gs_x + 2s_y)$, between the perpendicular and parallel polarized scattered light components, s_y and s_x, the absolute value of the anisotropy, r_S, corrected for the scatter contributions is given by eq 3.

$$r_S = \left[G(\sum_{v=1}^{k} c_{x,v}) - (\sum_{v=1}^{k} c_{y,v}) - \gamma\left(1 - \frac{3}{2}\alpha\right)c^{\Sigma}_{x,y,z}\right] \Big/ \left[(1 - 3l_2)G(\sum_{v=1}^{k} c_{x,v}) + (2 - 3l_1)(\sum_{v=1}^{k} c_{y,v}) - \gamma\left(1 - 3l_2 - \frac{3}{2}\alpha(l_1 - 2l_2)\right)c^{\Sigma}_{x,y,z}\right] \quad (3)$$

$$\text{with } c^{\Sigma}_{x,y,z} = G(\sum_{v=1}^{k} c_{x,v}) + 2(\sum_{v=1}^{k} c_{y,v})$$

Figure 2 depicts the experimental (dots) and theoretical (lines) dependence of the scatter-corrected steady-state anisotropy, r_S, on the number of detected fluorescence photons (burst size) for pure solutions of Rh 123 and EYFP on the single-molecule level for selected bursts (Figure 1). The corresponding probability densities of r_S (r_S(Rh 123) = 0.01 ± 0.05 (A) and r_S(EYFP) = 0.34 ± 0.06 (B)) are shown as projections in Figure 2. These results are in good agreement with steady-state ensemble measurements (Table 1) and with the values calculated from the Perrin equation (see below eq 4). The projection in Figure 2C shows a histogram of r_S, obtained from a mixture of

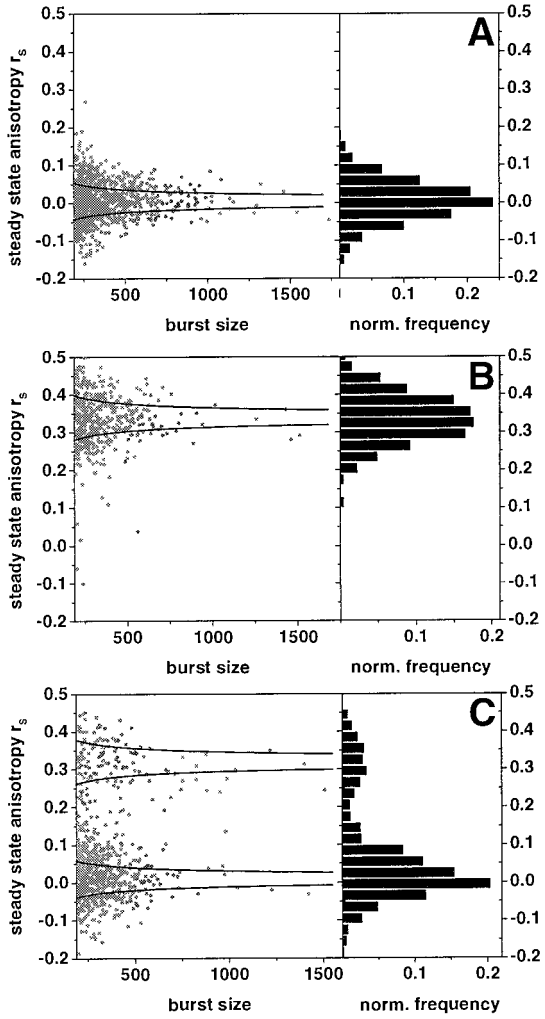

Figure 2. Experimental (dots) and theoretical (—) dependence of the scatter-corrected steady-state anisotropy, r_S, on the number of detected fluorescence photons (burst size) with the obtained probability densities of r_S given as a projection. (A) 1898 bursts of Rh 123, r_S(Rh 123) = 0.01 ± 0.05. (B) 578 bursts of EYFP, r_S(EYFP) = 0.34 ± 0.06. (C) 812 bursts of the mixture of both probe molecules, $r_{S1} = 0.01 \pm 0.05$ and $r_{S2} = 0.32 \pm 0.08$. The calculated theoretical standard deviation of r_S is based on the error propagation of parallel and perpendicular polarized fluorescence intensity.

TABLE 2: Optical Properties of the Fluorescent Probe Molecules Determined by the Probability Density of Single-Molecule Identification Using the Scatter-Polarization Ratio, α = 0.53, and the Correction Factors l_1 = 0.0308, l_2 = 0.0368, and G = 1.034 (eqs 2 and 3)

properties	Rh 123	EYFP	Rh 123 + EYFP	misclassification probability
τ	4.0 ± 0.4 ns	3.2 ± 0.4 ns		16%
r_E	0.03 ± 0.05	0.33 ± 0.05	0.04 ± 0.06 0.31 ± 0.08	3%
r_S	0.01 ± 0.05	0.34 ± 0.06	0.01 ± 0.05 0.32 ± 0.08	1%

Rh 123 and EYFP (concentration ratio: 4/1). Two clearly separated distributions of r_S can be seen. Thus, the anisotropy value of each single component is well recovered.

The influence of the scatter correction on the anisotropy is compared in Table 2. The scatter signal originates from Raman scattering from water and is slightly polarized (α = 0.53), yielding an anisotropy of pure background of r_E(scatter) = 0.26. Because the experimental anisotropies have the order r_E(Rh 123) < r_E(scatter) < r_E(EYFP), the inclusion of background signal

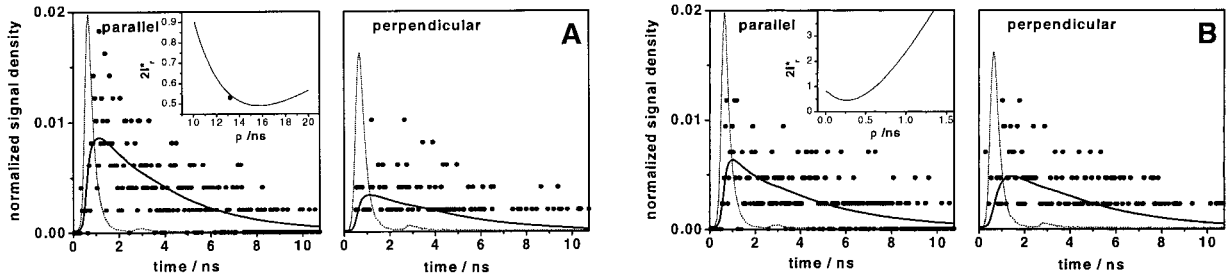

Figure 3. Parallel and perpendicular fluorescence decay components with respect to linear polarized excitation at 502 nm (A) for a single burst containing 500 photons (●) of EYFP and (B) for a single burst containing 425 photons of Rh 123. Instrument response function (- - -) and the global reconvolution fits (—) to both parallel and perpendicular fluorescence components are also shown (A: $\tau = 3.3 \pm 0.4$ ns, $\gamma = 0.03$, $r(0) = 0.39$ (fixed), $\rho = 15.7 \pm 1.4$ ns, $\alpha = 0.53$ (fixed). B: $\tau = 3.8 \pm 0.5$ ns, $\gamma = 0.01$, $r(0) = 0.37$ (fixed), $\rho = 0.3 \pm 0.5$ ns, $\alpha = 0.53$ (fixed)). The insets display the dependence of $2I_r^*$ on the rotational correlation time ρ.

has an opposite effect on the scatter correction of the fluorescence of Rh 123 and EYFP. Thus, the scatter correction results in a decrease of r_S(Rh 123) and an increase of r_S(EYFP) with respect to r_E (Table 2).

The efficiency of identification and classification of single Rh 123 and EYFP molecules via their characteristic steady-state anisotropy, r_S, is determined by the overlap of the two Gaussian distributions. Thus, the misclassification probability in identification of the fluorophores in the mixture amounts to only 1%. In contrast, the corresponding distributions of the fluorescence lifetimes obtained in single-molecule identification (τ(Rh 123) = 4.0 ± 0.4 ns and τ(EYFP) = 3.2 ± 0.4 ns) (data not shown) yield an overlap of 16%. This comparison demonstrates the significantly reduced misclassification probability based on anisotropy in identifying single molecules in a mixture of dyes with similar fluorescence spectra and lifetimes.

Time-Resolved Anisotropy. Within the spherical rotator model, the Perrin equation (eq 4) allows a molecular description of the steady-state anisotropy, r, by linking r to characteristic dynamic fluorescence properties described by lifetime, τ, and rotational correlation time, ρ, with the anisotropy, $r(0)$, at time zero.

$$r = \frac{r(0)}{1 + \tau/\rho} \tag{4}$$

Since BIFL allows simultaneous time-resolved fluorescence spectroscopy with two detectors, we present an algorithm for time-resolved anisotropy analysis of the arrival-time histograms in single-molecule spectroscopy. Due to the small number of detected fluorescence photons, a statistically efficient pattern recognition technique must be used. For data analysis, a synthetic signal pattern, m, is generated in several steps for the final comparison with experimental data, c. Note that capital letters are used for normalized data. m consists of the fluorescence, j, imaged by the objective and the prompt background, s (due to Raman and Rayleigh scattering), emerging from the microscope objective. A realistic fluorescence pattern, j, is obtained by convolution of the instrument response function, s (equal to the registered scatter), with a decay model function, j', taking into account the limited arrival time window, T, and the iterative excitation with the frequency, $1/\omega$.

$$j(\tau,\rho,T) = (\sum_{n=0}^{\infty}(s \otimes j')(t + n\omega)) \tag{5}$$

Depending on the analyzing detector, different decay model functions, j'_x and j'_y, must be used for fluorescence parallel to the x- and y-axis, respectively.[23]

$$j'_x(\tau,\rho) = \frac{j'(0)}{3}\exp(-t/\tau)[1 + r(0)(2 - 3l_1)\exp(-t/\rho)] \tag{6}$$

$$j'_y(\tau,\rho) = \frac{j'(0)}{3}\exp(-t/\tau)[1 - r(0)(1 - 3l_2)\exp(-t/\rho)] \tag{7}$$

Since the data are accumulated in k channels, the continuous time, t, in the signal decay patterns is once again later replaced by the time, $t_i = iT/k$, of the channel, i. The normalized fluorescence probability pattern, $J_{x,i}$ and $J_{y,i}$ in channel i is obtained by dividing $j_{x,i}$ and $j_{y,i}$ by the total fluorescence intensity. However, the normalized scatter probability patterns, $S_{x,i}$ and $S_{y,i}$ are calculated from $s_{x,i}$ and $s_{y,i}$ by dividing by the intensity registered by the respective detector.

$$J_{x,i}(k,\tau,\rho,T,s) = \frac{j_{x,i}}{\sum_{v=1}^{k} j_{x,v} + 2\sum_{v=1}^{k} j_{y,v}} \qquad S_{x,i}(T,s) = \frac{s_{x,i}}{\sum_{v=1}^{k} s_{x,v}} \tag{8}$$

$J_{y,i}$ and $S_{y,i}$ are defined in an analogous way. Considering the polarization ratio, α, and the background fraction, γ, the normalized model function, $D_{x,i}$ and $D_{y,i}$, in the channel i of the imaged signal is given by a sum of fluorescence, $J_{x,i}$ and $J_{y,i}$, and scatter, $S_{x,i}$ and $S_{y,i}$.

$$D_{x,i}(k,\tau,T,\rho,\gamma,\alpha,s) = (1 - \gamma)J_{x,i} + (1 - \alpha)\gamma S_{x,i} \tag{9}$$

$$D_{y,i}(k,\tau,T,\rho,\gamma,\alpha,s) = (1 - \gamma)J_{y,i} + \frac{\alpha}{2}\gamma S_{y,i} \tag{10}$$

To construct the final normalized decay pattern, $M_{x,i}$ and $M_{y,i}$, registered by the detectors, the G factor of the detection system must be taken into account.

$$M_{x,i}(k,\tau,T,\rho,\gamma,\alpha,s) = \frac{D_{x,i}}{\sum_{v=1}^{k}(D_{x,i} + GD_{y,i})}$$

$$M_{y,i}(k,\tau,T,\rho,\gamma,\alpha,s) = \frac{GD_{y,i}}{\sum_{v=1}^{k}(D_{x,i} + GD_{y,i})} \tag{11}$$

The optimal pattern, M_x and M_y, for a certain data set, c_x and c_y, is determined by global analysis with a maximum likelihood estimator procedure based on a product of two probabilities for a photon: (1) the probability to be registered by either detector one or detector two (binomial distribution) and (2) the probability to fall in channel i of the arrival-time histogram

(multinomial distribution). The quality of the fit is judged using the parameter, $2I_r^*$, (for details see refs 6 and 24−26).

$$2I_r^* = \frac{4k}{k-1-g}\left[c_x^\Sigma \ln\left(\frac{c_x^\Sigma}{p_x c_{(x,y)}^\Sigma}\right) + c_y^\Sigma \ln\left(\frac{c_y^\Sigma}{p_y c_{(x,y)}^\Sigma}\right)\right] + \frac{2}{k-1-g}\left[\sum_{\upsilon=1}^{k} c_{x,\upsilon} \ln\left(\frac{c_{x,\upsilon}}{c_{(x,y)}^\Sigma M_{x,\upsilon}(k,\tau,T,\rho,\gamma,\alpha,s)}\right) + \sum_{\upsilon=1}^{k} c_{y,\upsilon} \ln\left(\frac{c_{y,\upsilon}}{c_{(x,y)}^\Sigma M_{y,\upsilon}(k,\tau,T,\rho,\gamma,\alpha,s)}\right)\right] \quad (12)$$

Here, g is the number of fitted parameters, c_x^Σ, c_y^Σ, $c_{(x,y)}^\Sigma$ are the total numbers of the selected photons registered by the first, second, and both detectors (e.g., $c_x^\Sigma = \sum_{\nu=1}^{k} c_{x,\nu}$), respectively. $p_x = \sum_{\nu=1}^{k} M_{x,i}$ and $p_y = 1 - p_x$ are the probabilities of the model function to register a photon by detector one and detector two, respectively.

The fluorescence intensity emerging from the microscope objective, $j_{(x,y,z)}$, corrected for contributions from rotational dynamics to its time dependence is then for channel i given by the weighted sum of $j_{x,i}$ and $j_{y,i}$

$$j_{(x,y,z),i} = (1 - 3l_2)j_{x,i} + (2 - 3l_1)j_{y,i} \quad (13)$$

Under such magic-angle conditions, the fluorescence decay model function, $j'_{(x,y,z),i}$, is a single exponential, $j'_{(x,y,z),i}(\tau) = j'(0)\exp(-t_i/\tau)$, and the normalized pattern, $M_{(x,y,z),i}$, of the signal irrespective of molecular rotation is approximated by eq 14 reported by Brand et al.[6]

$$M_{(x,y,z),i}(k,\tau,T,\gamma,s) = (1-\gamma)J_{(x,y,z),i} + \gamma S_{(x,y,z),i} \quad (14)$$

Figures 3A and B show two typical signal decay curves of the x-polarized (detector 1) and y-polarized (detector 2) components together with the fitted patterns for a single fluorescence burst of EYFP and Rh 123, respectively. It is evident that in the case of EYFP the parallel fluorescence decay differs significantly from that of the perpendicular decay (A), whereas both decays are very similar for Rh 123 (B). This indicates marked differences in rotational correlation times, ρ, of EYFP and Rh 123, as expected from their respective mass and shape.

The data analysis was performed in two steps: (1) Fit to the fluorescence signal irrespective of molecular rotation using the pattern, $M_{(x,y,z)}$, of eq 14 to determine the fluorescence lifetime, τ, and the scatter fraction, γ, which were fixed in the next step. (2) Global fit (eq 12) to the data, $c_{x,i}$ and $c_{y,i}$, by the use of the patterns, $M_{x,i}$ and $M_{y,i}$ (eq 11), with the fluorescence decay model functions, j'_x and j'_y (eq 6 and 7), to determine the rotational correlation time, ρ.

There is clearly an intrinsic difficulty in measuring long rotational correlation times, ρ, from short fluorescence anisotropy decays, which appear in parallel and perpendicular record as $1/(\tau^{-1} + \rho^{-1})$ (eqs 6 and 7). In single-molecule spectroscopy, several experimental factors additionally limit the accuracy of the anisotropy parameters: (1) The time resolution of the detection system (FWHM of the instrument response function 400 ps) is determined by the avalanche photodiodes and exceeds the fitted value of $\rho \approx 300$ ps for a single burst of Rh 123 in water (Figure 3). (2) The arrival time window, T, set by the laser frequency is small (13.6 ns) compared with ρ(EYFP) ≈ 15.7 ns.[25] Because of the short lifetime, there is essentially no fluorescence left at 13.6 ns. Thus, the short time window is only a minor limitation in our case. (3) Due to the limited dwell time in the open detection volume, the number of detected photons for a single-molecule event in solution is small. Thus, under these conditions, it is advantageous to fix either $r(0)$ or ρ to values known from our own ensemble measurements (Table 1). Applying these prerequisites, our results give evidence that even under these suboptimal conditions, it is possible to obtain good estimates for the anisotropy parameters from these single-molecule measurements. We note that we perform many measurements on the individual molecule and average over more than 200 detected photons. Because our probe molecules rotate rapidly enough to sample all spatial orientations in the laser beam during their dwell time, the fundamental postulate of statistical mechanics can be applied for this homogeneous system, i.e., the time average is equal to the ensemble average.

Conclusions

In previous studies, single-molecule identification of various fluorophores has been based on sufficiently different lifetimes, without considering anisotropy.[2,3,5,8] However, multidimensional fluorescence spectroscopy presents the opportunity for using as many fluorescence parameters as necessary for an effective single-molecule identification. That is, besides lifetime and anisotropy, fluorescence count rates can also be used to monitor the relative fluorescence quantum yield of a single molecule, determined by emission and excitation characteristics. Recently, the fluorescence burst size and intraburst fluorescence lifetime were applied to a very precise identification of single molecules in flowing sample streams.[7] Even in the case of an open detection volume, we observe a difference of a factor of 2 between the relative burst count rates of Rh 123 and EYFP. If a single fluorescence parameter is not sufficient to conclusively distinguish between different molecular species in a mixture, the other parameters can be used for more precise identification. Thus, multidimensional fluorescence detection exploiting the fluorescence parameters anisotropy, lifetime, and quantum yield can decrease the misclassification probability of single-molecule identification. This is a major step toward a more detailed molecular recognition of different states of biomolecules, such as exhibited by single DNA dynamics.[10]

Acknowledgment. We are grateful to J. Troe and J. Wolfrum for support of this work. This work was supported by the Bundesministerium für Bildung und Forschung, Grant No. 0310806. A.V. acknowledges support from the Boehringer Ingelheim Foundation. V.S. is a recepient of a postdoctoral fellowship from the Human Frontiers Science Program Organization (HFSPO).

References and Notes

(1) Soper, S. A.; Davis, L. M.; Shera, E. B. *J. Opt. Soc. Am. B* **1992**, *9*, 1761−1769.

(2) Zander, C.; Sauer, M.; Drexhage, K. H.; Ko, D. S.; Schulz, A.; Wolfrum, J.; Brand, L.; Eggeling, C.; Seidel, C. A. M. *Appl. Phys. B* **1996**, *63*, 517−523.

(3) Müller, R.; Zander, C.; Sauer, M.; Deimel, M.; Ko, D. S.; Siebert, S.; Arden-Jacob, J.; Deltau, G.; Marx, N. J.; Drexhage, K. H.; Wolfrum, J. *Chem. Phys. Lett.* **1996**, *262*, 716−722.

(4) Keller, R. A.; Ambrose, W. P.; Goodwin, P. M.; Jett, J. H.; Martin, J. C.; Wu, M. *Appl. Spectrosc.* **1996**, *50*, 12A−32A.

(5) Enderlein, J.; Goodwin, P. M.; van Orden, A.; Ambrose, W. P.; Erdmann, R.; Keller, R. A. *Chem. Phys. Lett.* **1997**, *270*, 464−470.

(6) Brand, L.; Eggeling, C.; Zander, C.; Drexhage, K. H.; Seidel, C. A. M. *J. Phys. Chem. A* **1997**, *101*, 4313−4321.

(7) van Orden, A.; Machara, N. P.; Goodwin, P. M.; Keller, R. A. *Anal. Chem.* **1998**, *70*, 1444−1451.

(8) Fries, J. R.; Brand, L.; Eggeling, C.; Köllner, M.; Seidel, C. A. M. *J. Phys. Chem. A* **1998**, *102*, 6601−6613.
(9) Ha, T.; Enderle, T.; Chemla, D. S.; Selvin, P. R.; Weiss, S. *Phys. Rev. Lett.* **1996**, *77*, 3979−3982.
(10) Eggeling, C.; Fries, J. R.; Brand, L.; Günther, R.; Seidel, C. A. M. *Proc. Natl. Acad. Sci. U.S.A.* **1998**, *95*, 1556−1561.
(11) Ha, T.; Glass, J.; Enderle, T.; Chemla, D. S.; Weiss, S. *Phys. Rev. Lett.* **1998**, *80*, 2093−2096.
(12) Chalfie, M. *Photochem. Photobiol.* **1995**, *62*, 651−656.
(13) Misteli, T.; Spector, D. L. *Nature Biotech.* **1997**, *15*, 1−4.
(14) Miesenbock, G.; Deangelis, D. A.; Rothman, J. E. *Nature* **1998**, *394*, 192−195.
(15) Cubitt, A. B.; Heim, R.; Adams, S. R.; Boyd, A. E.; Gross, L. A.; Tsien, R. Y. *Trends Biochem. Sci.* **1995**, *20*, 448−455.
(16) Heim, R.; Tsien, R. Y. *Curr. Biol.* **1996**, *6*, 178−182.
(17) Delagrave, S.; Hawtin, R. E.; Silva, C. M.; Yang, M. M.; Youvan, D. C. *Biotechnology* **1995**, *13*, 151−154.
(18) Mitra, R. D.; Silva, C. M.; Youvan, D. C. *Gene* **1996**, *173*, 13−17.
(19) Mahajan, N. P.; Linder, K.; Berry, G.; Gordon, G. W.; Heim, R.; Herman, B. *Nature Biotech.* **1998**, *16*, 547−552.
(20) Ormo, M.; Cubitt, A. B.; Kallio, L. A.; Gross, L. A.; Tsien, R. Y.; Remington, S. J. *Science* **1996**, *273*, 1392−1395.
(21) Janknecht, R.; de Martynoff, G.; Lou, J.; Hipskind, R. A.; Nordheim, A.; Stunnenberg, H. G. *Proc. Natl. Acad. Sci. U.S.A.* **1991**, *88*, 8972−8976.
(22) Enderlein, J.; Robbins, D. L.; Ambrose, W. P.; Goodwin, P. M.; Keller, R. A. *Bioimaging* **1997**, *5*, 88−98.
(23) Koshioka, M.; Saski, K.; Masuhara, H. *Appl. Spectrosc.* **1995**, *49*, 224−228.
(24) Hall, P.; Selinger, B. *J. Phys. Chem.* **1981**, *85*, 2941−2946.
(25) Köllner, M. *Appl. Opt.* **1993**, *32*, 806−820.
(26) Köllner, M.; Fischer, A.; Arden-Jacob, J.; Drexhage, K. H.; Müller, R.; Seeger, S.; Wolfrum, J. *Chem. Phys. Lett.* **1996**, *250*, 355−360.